PIV of Flow Convection Induced by Solar Sphere to Generate Power

Hassan Abdulmouti
Associate Professor, Department of Mechanical Engineering Division
Sharjah Men's College, Higher Colleges of Technology
Sharjah, UAE
e-mail: habdulmouti@hct.ac.ae, alternative e-mail: hassanabujihad@hotmail.com

***Abstract*—Flow visualization including image processing and Particle Image Velocimetry (PIV) measurements is used to evaluate the flow velocity field of the acrylic solar sphere filled with oil. This generated convection flow is affected by the thickness of the sphere, the sphere size as well as the temperature. The function of the acrylic sphere which is a modern technology of concentrated photovoltaic is to gather the energy from the sun and then concentrate it in a compact area like a focal spot. This focal spot is placed and put directly above a multi-junction device that acts as a concentrator cell appliance. This appliance directly can generate an enormous rate of power that is utilized to generate more electricity rather than the power that normal photovoltaic panels (PV) can produce. The acrylic sphere is used also for a lot of industrial applications. This research paper aims to investigate the characteristics of the flow inside the sphere and explore the sphere thickness, the sphere size, and the sphere temperature effect on the flow velocity of the fluid motion. Moreover, the purpose of this study is to clarify the relationship between these parameters in order to achieve greater efficiency for power generation, therefore, improve its performance. The results showed that the sphere thickness, the sphere temperature, and the sphere size significantly change the flow structure value. It is found that the velocity increase as the sphere thickness decreases. Hence, the efficiency of the sphere increases when using lower acrylic sphere thickness, higher size, and lower liquid temperature. The output power and efficiency of the solar sphere increase with lower sphere thickness. The thinner the thickness of the acrylic layer, the higher the sunlight absorbed by the acrylic photons. Subsequently, the higher the output power, which results to get higher the efficiency.**

Keywords- PIV; Solar, Flow; Concentrate; Energy.

I. INTRODUCTION

Several threats to food security, water resources, and the environment have appeared and expanded, resulting in a strong demand for technological advancements in the energy sector. This is also reinforced by data demonstrating the exponential rise in power and energy research over the previous few decades. Parallel to this, energy demand is expected to rise to a high between 2016 and 2040 [1]-[3].

Despite the global expansion of trends favoring energy conservation, green energy supply, and low environmental effect, producing enough energy to meet global demand remains a tough task. The most difficult task remains to deliver power from clean sources, such as renewable energy, which can lead to a reduction in the use of fossil fuels [4]-[6].

Renewable energy's capacity to meet the world's energy needs is promising, and it has the potential to reduce reliance on traditional energy sources, such as oil and uranium. Because traditional energy sources are both expensive and harmful to the environment, renewable energy sources provide a competitive option for power generation. Among the different renewable energy sources, solar energy is the most abundant and easily available to cover human electrical usage. As a result, numerous researchers have been looking for novel ways to gather solar energy and use it as a renewable energy source [7]-[9].

The efficiency of the solar sphere which is a new technology is significantly higher than normal solar panel collector components. Following the introduction of solar panels, many sun lights concentrated systems have arisen. One of these is the solar sphere collector, which is more efficient than traditional solar panels. Other benefits of the solar sphere include a) the ability to convert solar energy directly into electrical energy, b) solar radiations can be collected at any angle, unlike conventional solar panels, which must be integrated with a tracking system in order to capture the maximum amount of solar radiations, and c) their size is smaller compared to conventional solar panels, which occupy larger areas for relatively the same amount of solar radiations [10][11].

The concentrated solar sphere system consists of an acrylic sphere filled with a fluid that absorbs sunlight and transforms it directly into electrical energy. This is accomplished by concentrating solar energy from all across the sphere and focusing it in a small focused area on a high-efficiency solar cell. A pyranometer is used to measure sun irradiance, while a multimeter is used to measure the electrical power generated by the solar cell.

The solar sphere collector technology was already investigated and tested in our past study. The trials included different spherical materials, sphere shapes, and sphere sizes, as well as different fluids. Numerous tests were conducted at various circumstances throughout the year in order to acquire and assess the power production and related efficiency corresponding to the various parameters compared to the traditional solar panel (PV). Based on prior studies, the solar sphere displayed superior power production and efficiency when compared to the standard solar panel for the various parameters that were tested. In addition to this finding, the following conclusions were reached:

 ISBN: 978-1-68558-054-4

1. When compared to other shapes using the same fluid, the entire spherical produced the most power. The power was nearly four times that of a regular solar panel.

2. Increasing the size of the solar sphere increases power production and the associated efficiency.

3. In terms of the fluid used to fill the solar sphere, oil had a maximum power output that was 1.5 times that of alcohol. Alcohol, on the other hand, produced double the power output of water, with air producing the least power production of the fluids, tested [12]-[15].

Convection flow is the flow of fluid within the solar sphere, and it is found in a variety of applications, such as oil and natural gas transport, column reactor, air-sea gas transfer, ship hydrodynamics, boiling heat transfer, and bubble column reactors [16]-[19]. Researchers are interested in such convection flows because they occur in many engineering applications and numerical research and experiments aid in visualizing and understanding the parameters involved in this movement. Understanding and clarifying the flow parameters assist in defining the flow behavior and investigating the efficacy of the flow to improve the flow behavior towards the region of interest of the application at hand [20]-[22].

The goal of this research is to examine and comprehend the properties of flow in the solar sphere through the analysis of the velocity of fluid flow within the solar sphere using PIV. Furthermore, to investigate the influence of sphere thickness, sphere size, and sphere temperature on fluid motion and velocity. Furthermore, in order to increase the performance of the system to generate power and then maximize its efficiency, the link between these factors must be well defined.

In Section 2 of this paper the experimental apparatus and methods were illustrated. While in Section 3 the flow visualization and image processing results, including the PIV system and data analysis were explained. The conclusion was added in Section 4.

II. Experimental Methods and Apparatus

Figure 1 depicts the setup of the intended experiment. The acrylic (Plexiglas) solar sphere (No.1) material gives optical access, to the flow inside the sphere, to facilitate observation as well as image processing via PIV measurements and permits the collection of the solar radiation necessary to be focused. The sphere is full of frying oil (sunflower oil). The sphere is supported by a stainless-steel stand (No. 2).

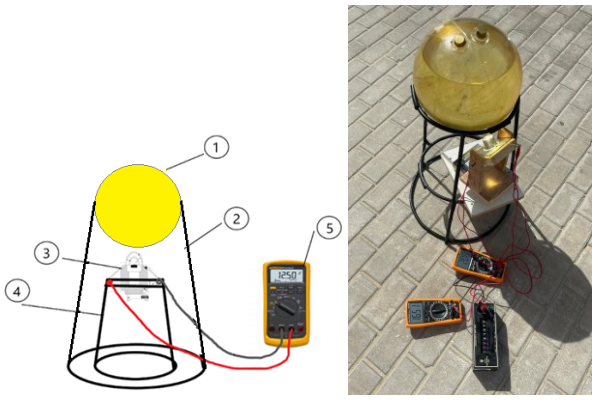

Figure 1. The setup for the solar sphere experiment.

A multi-junction concentrator solar cell (No. 3) is mounted on a stand (No. 4) beneath the solar sphere and is directly linked to a multi-meter (No. 5) to measure power production by measuring voltage and current ampere.

The solar sphere collects solar energy from the sun and focuses it on a single point. This focus point is located on top of a collector device, which is a multi-junction cell. The magnifying lenses in the multi-junction cell arrangement focus the solar radiations onto a focused region in the cell. This concentrated region is linked to a heat sink. The multi-junction cell is further subdivided into sub-cells, each of which is in charge of converting distinct components of the light into electricity. Because this device can withstand high temperatures and can help in radiation resistance, it was chosen to be utilized in this experiment to capture the concentrated solar energy of the focus point. The multi-junction device is connected to a multi-meter, which is used to read the output current and voltage. The experiment setup utilized to investigate flow characterization using flow visualization and image processing via PIV measurements consists of the apparatus shown in Figure 2 which is listed below:

1- As a light source, a Mini Diode-pumped solid-state laser (DPSS) Model #SM-SEMI-2W, which is a double pulse laser (also known as PIV laser), is employed. It employs two pulse lasers to emit laser beams via an optical beam combiner and a light path exit. The wavelength of the laser is 532 nm.

2- The CCD scientific class digital camera, Model #SM-CCDB2M25, records the visualized flows. This camera uses a double exposure mode that is coordinated with the double laser pulses and has a 50 mm f/1.4, F-Mount Lens, Model #SM-LENS5014. An external trigger initiates the capture. The frame grabber then sends both collected pictures to computer memory in real-time. A synchronizer generates trigger signals that are properly synced with the double-pulsed laser. The camera has a resolution of 1620×1220 (2M) and can take 25 frames per second (or 12.5 image pairs). The minimum exposure time interval in PIV mode is 200ns.

3- The synchronizer with USB cable, Model #MicroPulse 825 (MicroPulse725), provides cycle pulse trigger signals via the internal time base while also creating numerous delayed trigger signals via internal time-delay channels. The synchronizer is used to regulate the laser, digital camera(s), and frame grabber, ensuring that all of these diverse pieces function in perfect synchronicity.

4- A computer that is used to store picture data that has been captured by the frame grabber. It is then used by the Particle Image Velocity measurement system software to compute, display, and save the velocity field in real time.

5- The PIV system, which is 2D PIV software with particle image capture and velocity analysis, employs a laser as an independent illumination source that may be employed with or without the synchronizer. If the synchronizer is not accessible, the laser's internal synchronization can be used throughout the optical path and laser energy setup. Also employed is a high-resolution 2D2C PIV with multi-pass, multi-grid, window deformation method, and boundary deformation parameters. The frame grabber occupies a regular PCI (PCI-E) slot on the computer. The acquisition board's interface is primarily a 26-pin CamLink standard digital

 ISBN: 978-1-68558-054-4

camera connection interface. Digital cameras with a standard CamLink interface are used in the Microvec PIV system. It connects to the frame grabber through three 10-meter signal lines, retains trigger signals to synchronize the digital cameras with the pulse laser, and then links to the synchronizer's output interface via coaxial signal cables via TTL trigger, which interfaces with the camera. When the synchronizer is provided as part of the PIV system, the laser must be set to external synchronous mode (where the synchronizer's 4-way delay signals are output to controls of the corresponding two sets of the laser flashlamp and Q-switch) while the digital camera is set to PIV work mode.

6- Fluorescent spherical tracer particles Model #MV-H1020 with a diameter of 7 µm (mean 10 µm) and a density of 1.04 - 1.06 g/cc are used as tracer particles to see the flow and determine velocity vectors.

As previously stated, the PIV measurements are employed in this study to produce the findings, which collect and calculate the velocity/velocity vectors of the flow inside the solar sphere, including flow visualization and image processing. To perform the tests within the lab, a lighting arrangement of 500 W Halogen lights is employed as a simulator instead of the sun. The laser is utilized with a black back sheet background to improve visibility and take high-quality photographs of the experiments for flow visualization and velocity measurements.

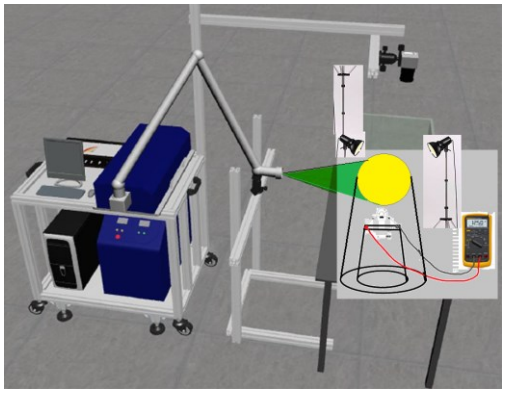

Figure 2. PIV Experimental Configuration

III. Flow visualization and image processing results, including the PIV System and Data Analysis

Particle Image Velocimetry (PIV) is an optical flow imaging technique. It made use of the acquired instantaneous velocity measurements as well as the related fluid characteristics. Tracer particles must be introduced into the fluid to help in the capture of velocity vectors. The velocity vectors will be generated by lighting the region of interest with the laser and then monitoring the seeded particles. The tracer or seeded particles are supposed to follow the motion of the fluid, which is evenly dispersed throughout the flow field, and the interrogation window, which has a distinct speed. When the tracer particles are in motion, their flow is caught by sequential imaging, which is then processed for additional cross-correlation, allowing the observed flow's speed and direction (the velocity field) to be calculated. Furthermore, additional processing may be performed using the flow vortices, flow field parameter distribution, speed lines, and flow lines. The configuration of a typical PIV system typically consists of four basic physical components. The digital CCD or CMOS camera is the first. The laser and its optical arrangement, which restricts the physical lit region of interest, are the second component. The third component is the synchronizer, which functions as an external trigger for regulating and timing both laser and cameras. As previously stated, the seeding particles are the fourth component. Of course, all of these components must be employed in conjunction with the fluid under investigation. The laser can be linked to specific lenses to transform the laser beam into a sheet or line ray. Finally, the optical pictures collected will be processed using specialist PIV software. The tracer particles following the movement of the fluid are emitted by the pulsed laser within the known time interval t, and the sheet light illumination by the lens group records the particles' instantaneous position on the CCD chip. If we know the displacement change of the same particle micelle at two times t1 and t2 from the recorded particle picture, we can calculate the velocity of the particle group at t1 using the definition of velocity, as indicated in the formula below [23]-[29].

$$v = \lim_{\Delta t \to 0} \frac{\Delta s}{\Delta t}$$

To begin analyzing the obtained picture, the idea of interpretation area must be defined. It refers to a square picture of a specific size in a specific location in the image, and the speed is acquired by executing signal processing in the interpretation area. Assume the system captures images 1 and 2 in Figure 3 at two different times, t_0 and t_{0+t}. Obtaining two interpretation regions of the same size, f(m,n), in the same spot in the picture. where (m, n) denotes the relative location of f and g in images 1 and 2, respectively. Processing f and g yields the appropriate displacement S of the interpretation area, as indicated in Figure 3.

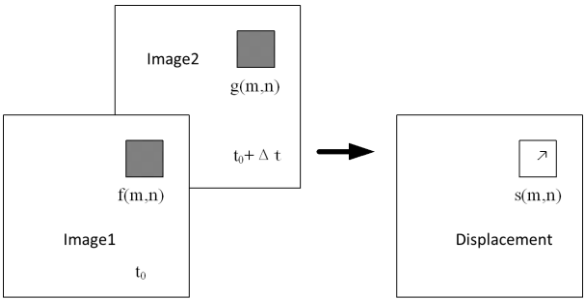

Figure 3. The system obtains images 1 and 2.

Figure 4 depicts the link between the digital signal transfer function and the interpretation regions f, g, and the displacement vector (the uppercase letters in the figure correspond to the lowercase Fourier transform). TSI's INSIGHT 4G® software is also utilized for picture and correlation analysis. The technique begins by analyzing the pictures using 6464 Interrogation Areas (IAs) using a Fast Fourier Transform (FFT) correlator, resulting in a 50% overlap of the interrogation areas. The correlation peak is then examined to acquire the findings of the final questioning region of 1616 pixels in size. The Gaussian curve-fitting approach with subpixel precision is used to determine this. The median technique, one of the post-

processing methods available in the TSI analysis program, is used to remove spurious vectors from velocity fields. The rejection rate of the vectors is roughly 3%. The Gaussian-weighted technique replaces these rejected vectors with their neighbors [30]-[34].

In the applied image processing, an average duration of 10 µs consecutive frames (between 2 consecutive frames) is utilized to discover the values of the velocity of the flow inside the spheres of 10 cm 15 cm, and 30 cm diameters, and for different thicknesses of 3, 4, 5, 6 and 8 mm. These experiments are conducted for 3 different temperature rates of 35, 40, and 45ºC. The velocity is determined and then computed for all these spheres/cases. Image processing calculates the flow velocity estimate at roughly 10,000 vectors of the flow pictures. The velocity experiments are carried out for the entire sphere. For each example, the temperature, voltage, and current ampere were measured, hence the output power was determined.

Figure 5 depicts a sample of images of the sphere with a diameter of 15 cm and a thickness of 8 mm, whereas Figure 6 depicts a sample of flow images for the experimental acrylic sphere with a diameter of 10 cm and a thickness of 4 mm illuminated by laser for flow visualization and further image processing for velocity size computations.

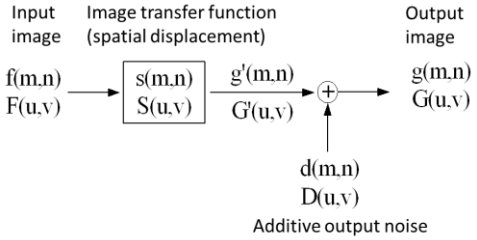

Figure 4 The connection between the interpretation regions f and g

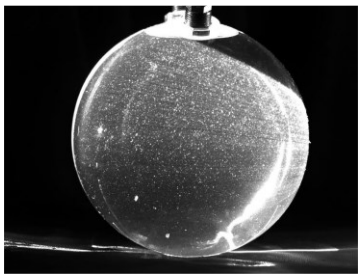

Figure 5. Images of a sphere with a diameter of 15 cm and 8 mm thickness

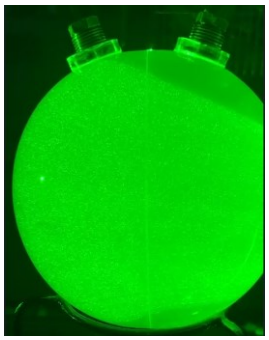

Figure 6. Images of an experimental laser-illuminated acrylic sphere with a diameter of 10 cm and a thickness of 4 mm

Figure 7 shows a PIV vector plot with an instantaneous velocity field (vectors sample) of the flow within the sphere of 15 cm diameter and 3 mm thickness at a temperature of 35ºC measured by PIV between the first frame and frame number 200 in order to easily distinguish the flow inside the sphere since the flow is quite sluggish. Figure 8 illustrates a sample of the immediately dispersed velocity vector of the flow in a sphere of 15 cm diameter and 5 mm thickness measured by PIV between the first and 80th frames at a temperature of 35ºC. Figure 9 illustrates a sample of the immediately dispersed velocity vector of the flow in a sphere of 15 cm diameter and 8 mm thickness measured by PIV between the first and frame number 200 at a temperature of 35ºC. Figure 10 demonstrates the result of the flow visualization and vorticity of the flow in the sphere of 10 cm diameter and 6 mm thickness measured by PIV between the first and the 40th frame at a temperature of 45ºC.

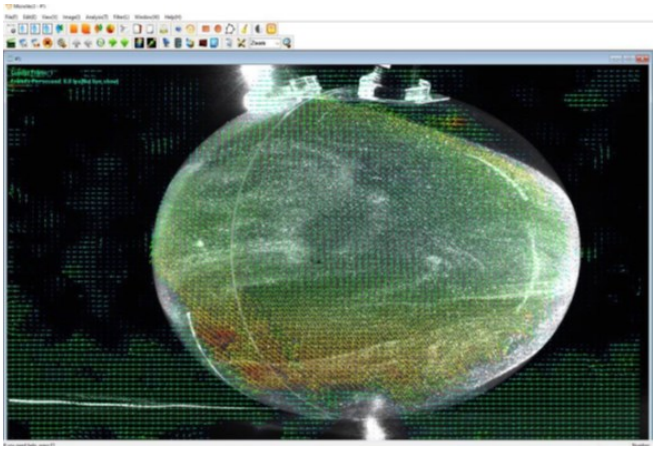

Figure 7. PIV recorded an instantaneous velocity vector sample of the flow in a sphere of 15 cm diameter and 3 mm thickness (1-200 frame) at a temperature of 35ºC.

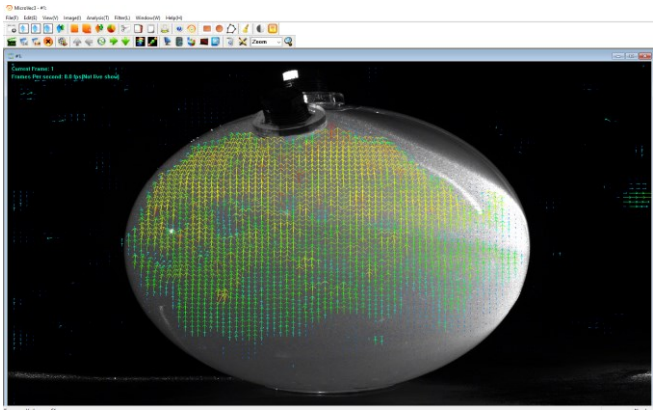

Figure 8. PIV recorded an instantaneous velocity vector sample of the flow in a sphere of 15 cm diameter and 5 mm thickness (1-80 frame) at a temperature of 35ºC.

The velocity of the fluid (particles) at the top of the sphere is clearly higher than the velocity of the seeded particles in other regions of the fluid motion, as shown by these figures. Because there are many interaction types between the flow of the liquid and the upper part of the inside wall of the sphere, the flow generated on the top of the sphere is considered an appropriate technique that aids in the detailed investigation of the flow regime during the

 ISBN: 978-1-68558-054-4

flow motion from the bottom of the sphere to the top of the sphere. Furthermore, the liquid flow characteristic at the top region does not behave similarly to other flow regions. This is because the fluid flow on the top reaches the upper wall and reacts with it by mirroring the direction downward. As a result, the upper half of the spherical wall guides, directs, and reflects the fluid flow, whereas the flow in other places delays the fluid. Actually, the interaction between the fluid flow and the spherical wall is extremely evident. As a result, this inquiry and its accompanying data assist in determining the entrainment flow in the downward direction. This also encourages research into the relative velocity expression and its reaction and flow behavior to the encirclement liquid.

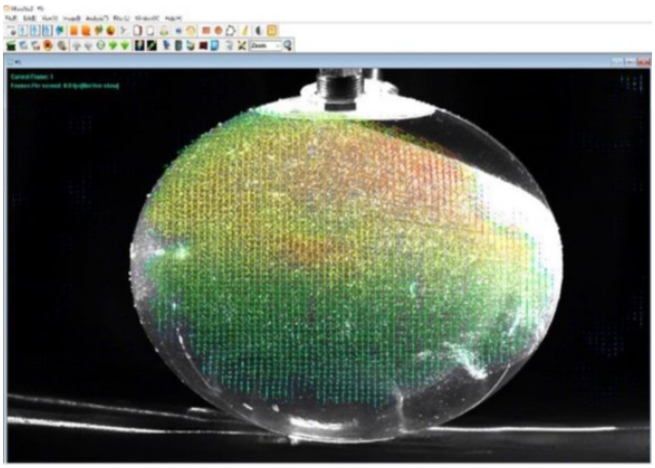

Figure 9. PIV recorded an instantaneous velocity vector sample of the flow in a sphere of 15 cm diameter and 8 mm thickness (1-200 frame) at a temperature of 35ºC.

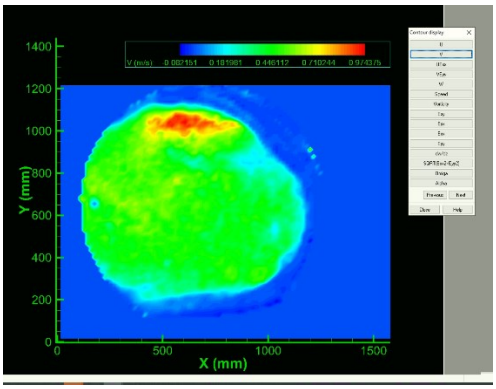

Figure 10 Result of the flow visualization and vorticity of the flow in the sphere of 10 cm diameter and 6 mm thickness (1-40 frame)

The complete explanation of the flow process within the sphere may be presented and summarized using the resulting figures as follows. The produced convection flow pattern is equally harmonic around the sphere center, where the movements were primarily caused inside the fluid as a result of the tendency of the fluid with higher temperature and lower density to rise and the fluid with lower temperature and higher density to sink with the effect of gravity, resulting in heat transfer. Furthermore, the flow is observed to be steady and uniform around the center, with the exception of the region of the top surface where the fluid flow impinges and reflects. The rising flow around the center is steered by the sphere's wall, resulting in a significant fluid flow formation towards the upper region of the sphere. The flow evolves as follows: the maximum velocity for the upward flow momentum is obtained towards the upper top region of the sphere. When it is reflected downhill on the wall, the orientation of the upward flow changes quickly from an upwards direction to a downward direction flow. Following the formation of two circular liquid currents around the center, and after a specific amount of time has passed, those circular currents encourage the center of the sphere with a scale circulation throughout the complete fluid layers.

Figures 11, 12, and 13 show the relationship between the sphere thickness of 10 and 14, and 30 cm diameter and the fluid velocity for different temperatures of 35, 40, and 45ºC and for a sphere thickness of 3, 4, 5, 6, and 8 mm. The fluid velocity is calculated to be the average velocity of the top region under the wall surface. Because this is the more complicated area where the fluid has many interactions with the upper surface.

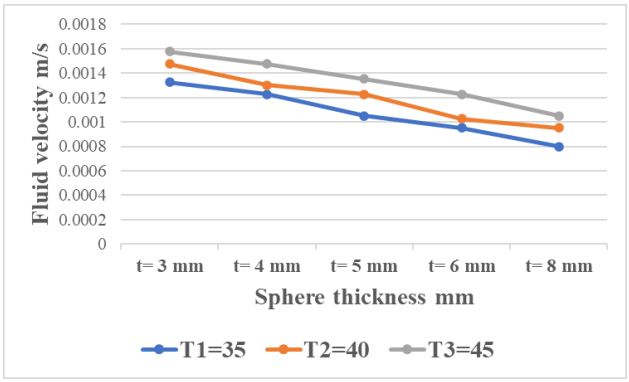

Figure 11 The relationship between the sphere thickness and the fluid velocity for different temperatures and for a sphere diameter of 10 cm

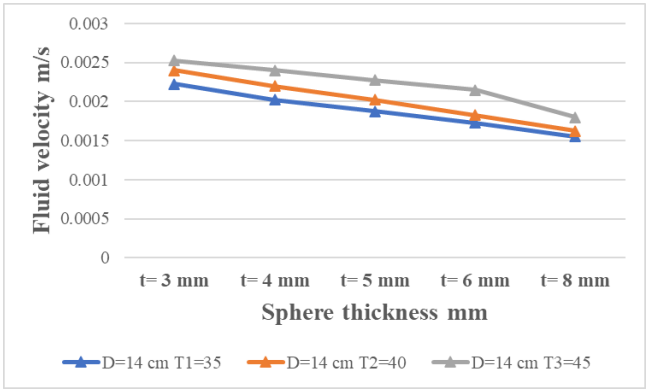

Figure 12 The relationship between the sphere thickness and the fluid velocity for different temperatures and for a sphere diameter of 14 cm

Figure 14 illustrates the relationship between the sphere thickness of 10 cm diameter with the output power and efficiency for a temperature of 35ºC and for a sphere thickness of 3, 4, 5, 6, and 8 mm. The current-voltage characteristics were plotted for each sphere thickness of 3, 4, 5, 6, and 8 mm separately. The optimum operating point is at the maximum power point. The values of these maximum power points were accumulated in Figure 14, It is clear from this figure that the output power and efficiency increase when using lower acrylic thickness. Hence, using a 3 mm sphere thickness is the best.

 ISBN: 978-1-68558-054-4

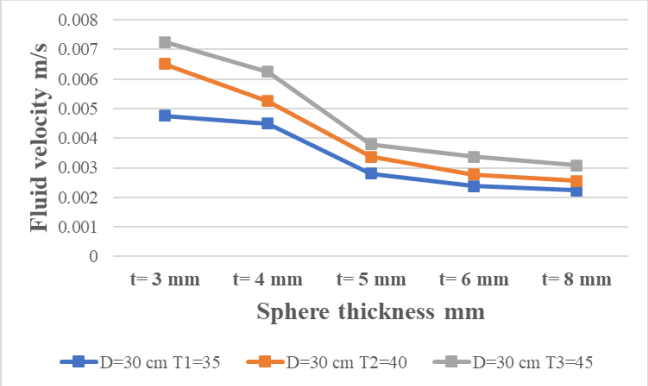

Figure 13 The relationship between the sphere thickness and the fluid velocity for different temperatures and for a sphere diameter of 30 cm

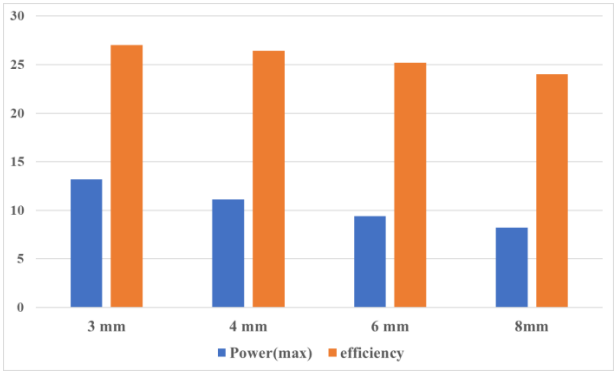

Figure 14 the relationship between the sphere thickness of 10 cm diameter and the output power and the efficiency for a temperature of 35ºC

According to the figures, the fluid flow approaches the top spherical surface as the velocity increases. Furthermore, when comparing the velocity vectors, it is discovered that when the spherical thickness lowers, the velocity increases. Whereas the average velocity of the 4 mm thickness sphere is nearly double that of the 6 mm thickness sphere in the region of the top surface of the sphere, and the average velocity of the 6 mm thickness sphere is nearly double that of the 8 mm thickness sphere in the region of the top surface of the sphere. Also, as the temperature increases the fluid velocity increases. Moreover, when the size of the sphere increases the fluid velocity also increases. Furthermore, it is acknowledged that the output power and the efficiency of the 4 mm thick sphere are greater than that of the 6 mm thick sphere. In reality, as the thickness of this acrylic solar sphere rises, the amount of solar radiation received is influenced and limited, becoming less. As a result, the output power is decreased. Hence, the greater the thickness of the acrylic, the less electricity is produced by the sun. When the thickness is reduced, more power is produced, resulting in improved efficiency. As a result, the thinner the acrylic coating, the more solar light is absorbed by the PV photons. As a result, the larger the output power, the higher the efficiency.

Finally, the behavior of flow motion within the solar sphere was explored in an attempt to improve power generation performance. The examination in this research effort was carried out to understand the influence of sphere thickness on fluid flow, which is elucidated in this document, in order to increase fluid flow performance and, hence, maximize the related efficiency. The results revealed that the thickness of the sphere considerably alters the flow structure and fluid velocity value. As a result, a thinner sphere should be employed to increase the efficiency of the solar sphere. Furthermore, the thinner the acrylic coating, the more sunlight is absorbed by the PV photons. As a result, the larger the output power, the higher the efficiency.

IV. CONCLUSIONS

The flow visualization and image analysis using PIV measurements on the fluid flow within a solar sphere and the velocity motion of the filled oil fluid were carried out in this study to optimize the flow behavior. The flow velocity and its influence on sphere thickness are calculated. The collected findings demonstrated a clear influence of spherical thickness and temperature on fluid flow. The following is an overview of the key conclusions:

1. The output power and efficiency increase when using lower acrylic thickness. Hence, using a 3 mm sphere thickness is the best.
2. When the temperature increases the fluid velocity increases and when the size of the sphere increases the fluid velocity also increases
3. The fluid flow velocity was discovered to grow and climb in value to the upper surface wall of the sphere, the mean velocity magnitude was determined, and it was discovered to be greater in the region of the top surface than the starting velocity in the other regions.
4. The fluid velocity data showed that the velocity increases as the thickness of the sphere decreases, and the mean velocity magnitude progressively increases as one rises within the sphere.
5. The output power and the associated efficiency of the solar sphere increase with respect to the properties of lower sphere thickness. The thinner the thickness of the acrylic layer, the higher the sunlight absorbed by the PV photons. Subsequently, the higher the output power, which results to get higher the efficiency.

ACKNOWLEDGMENT

The study described in this publication was supported by the Internal Interdisciplinary Research Grant No. (212194), Fund number 113180. HCT stands for High Colleges of Technology in the United Arab Emirates.

REFERENCES

[1] H. Abdulmouti, K. Ali, A. Ali, M. Ali, S. Abdullah, R. Abdalla, “Smart Innovation Applications for a GreenHouse Using Sustainable and Renewable Energy in the UAE,” Publisher: IEEE. DOI: 10.1109/ICASET.2018.8376782, Electronic ISBN: 978-1-5386-2399-2, Print on Demand (PoD) ISBN: 978-1-5386-2400-5, IEEE Xplore Digital Library: 11 June 2018.

[2] H. Abdulmouti, Z. Skaf, and S. Alblooshi, "Smart Green Campus: The Campus of Tomorrow," 2022 Advances in Science and Engineering Technology International Conferences (ASET), 2022, pp. 1-8, DOI: 10.1109/ASET53988.2022.9735087, Publisher: IEEE. Date Added to IEEE Xplore: 18 March 2022.

 ISBN: 978-1-68558-054-4

[3] O. Edenhofer, R. Pichs-Madruga, Y. Sokona, K. Seyboth, S. Kadner, T. Zwickel, & P. Matschoss, (Eds.), "Renewable energy sources and climate change mitigation: special report of the intergovernmental panel on climate change," Cambridge University Press, [Accessed 15 March. 2017].

[4] H. Abdulmouti, "Passive Cooling Module to Improve the Solar Photovoltaic (PV) Performance," The 4th Int. Conf. on Environment, Chemical Engineering & Materials. Athens, Greece, December 27-29, 2022. Published on WSEAS Transactions on Power Systems, vol. 18, pp. 11-17, 2023.

[5] Green Facts, "Forests & Energy: 2, What are the trends and prospects of energy supply and demand?," [Accessed 3 March. 2017].

[6] H. Abdulmouti, "Innovative Environment-Friendly Systems for a Modern Town," 12th International Conference on Sustainable Energy & Environmental Protection (SEEP'19), 18-21 Nov. 2019, UOS, Sharjah, UAE.

[7] H. M. Cooper, "Organizing knowledge syntheses: a taxonomy of literature review," Knowledge Society, 1, 104-126, [Accessed 3 March. 2017].

M. Marsal-Llacuna, J. Colomer-Llinàs, J. Meléndez-Frigola, "Lessons in urban monitoring taken from sustainable and livable cities to better address the Smart Cities initiative," Technological Forecasting and Social Change,Volume 90, Part B,2015,Pages 611-622, January 2015,

[8] V. Quaschning, "Renewable Energy and Climate Change," Berlin University of Applied Systems HTW, Germany, (Translator) Hedy Jourdan, A John Wiley & Sons, Ltd., Publication, 2010.

[9] Green Rhino Energy, "Concentrating Photovoltaics Solar Power," Retrieved May 06, 2016. http://greenrhinoenergy.com/solar/technologies/pv_concentration.php

[10] P. Salmerón Revuelta, S. Pérez Litrán, J. Prieto Thomas, "Design, Simulation and Implementation for Improving Power Quality," Distributed Generation, Academic Press, pages 285-322, ISBN 9780128032169, https://doi.org/10.1016/B978-0-12-803216-9.00008-0, 2016.

[11] H. Abdulmouti, "An Experimental Innovative Solar Sphere Design to Generate Electricity," 5th International Conference on Renewable Energy and Development (ICRED 2019), 20- 23 September 2019, Okinawa, Japan.

[12] H. Abdulmouti, A. Ahmed Aljasmi, M. Ali Almarzooqi, H. Alyasi, M. Jassim Khair, Y. Mohamed Almulla, A. Ahmed Almulla, "Generating Power from Innovative Solar Sphere," DOI: 10.1109/ICASET.2019.8714441, ISBN Information: Electronic ISBN: 978-1-5386-8271-5, Print on Demand (PoD) ISBN: 978-1-5386-8272-2, Date of Publisher: 16 May 2019, Publisher: IEEE Xplore.

[13] H. Abdulmouti, Producing Electricity by Concentrated Solar Energy," The 2nd International Conference on Advances in Energy Research and Applications (ICAERA'21), November 24 - 26, 2021, Seoul, South Korea.

[14] H. Abdulmouti, Z. Skaf, S. Alblooshi, S. Almheiri, "Exploring the Flow of Solar Sphere Using PIV," 5th Advances in Science and Engineering Technology multi-conferences (ASET 2023), International Conference on Sustainable Environment and Urban Infrastructure, "in press", 20-23 Feb. 2023.

[15] H. Abdulmouti, "Numerical Simulation of Bubble Convection in Two-phase Stratified Liquids," Multiphase Science and Technology by Begell House, Inc "USA", Volume 31, Issue 2, pp.:133–149 (2019), The Home for Science and Engineering, DOI: 10.1615/MultScienTechn.2019029995.

[16] H. Abdulmouti, "Experimental Measurement for Surface Flow Characteristics Generated by a Bubble Plume," The Journal of Flow Visualization and Image Processing, 22 (1–3), 39–58, 2015, Begell House "USA", The Home for Science and Engineering.

[17] H. Abdulmouti, "Experimental Measurements of Bubble Convection Models in Two-phase Stratified Liquids," Experimental Thermal and Fluid Science, Volume 83C, May 2017, pp. 69-77, (ELSEVIER), https://doi.org/10.1016/j.expthermflusci. 2016.12.010.

[18] H. Abdulmouti, "Bubbly Two-Phase Flow: Part II-Characteristics and Parameters," DOI: 10.5923/j.ajfd.20140404.01 American Journal of Fluid Dynamics, Volume 4, Number 4, 4(4): 115-180, December 2014, (Scientific and Academic Publishing).

[19] H., Abdulmouti, "Bubbly Two-Phase Flow: Part I-Characteristics, Structures, Behaviors and Flow Patterns," American Journal of Fluid Dynamics, Scientific and Academic Publishing, vol. 4, no. 4, 4(4), pp. 194-240. DOI: 10.5923/j.ajfd.20140404.03. December, 2014a.

[20] H., Abdulmouti, "The Measurements of Bubble Plume Structure Parameter," International Journal of Fluid Mechanics Research, Begell House "USA", The Home for Science and Engineering, 44(3): 1–19, 1064–2277/17/$35.00, 2017.

[21] H. Abdulmouti, "Measurements of Thermal Effect on Bubble Parameter," The 3rd Thermal and Fluids Engineering Conference (TFEC), March 4-7, 2018, Fort Lauderdale, FL, USA.

[22] H. Abdulmouti, "Particle Imaging Velocimetry (PIV) Technique: Principles, the typically used methods, classification and applications," Scholar's Press. ISBN-13: 978-3-639-51249-6, 6 March 2013.

[23] H., Abdulmouti, "2D- numerical simulation of surface flow velocity and internal flow structure generated by bubbles," Multiphase Science and Technology, Begell House (USA), the Home for Science and Engineering, 28 (2): 153–171, 0276–1459/16/$35.00 © 2016, DOI: 10.1615/MultScienTechn.2017018926, 2016.

[24] H. Abdulmouti, "Measurement of Flow Structures Induced by a Bubbly Plume Using Visualization, PIV, and Image Measurement," Scholar's Press, Saarbrücken, Germany, ISBN-13: 978-3-639-51490-2, 7, June 2013.

[25] R. Bastiaans, "Cross-correlation PIV : theory, implementation and accuracy," Compustion Technology, 4, 2000.

[26] H. Abdulmouti and M. Shinneeb, "Investigation of Free-Surface Flow Induced by a Bubbly Plume Using PIV," 2020 (ASET), Electronic ISBN: 978-1-7281-4640-9. ISBN: 978-1-7281-4641-6. Print on Demand (PoD), pp. 1-5, DOI: 10.1109/ASET48392.2020.9118203, Publisher: IEEE. Added to IEEE Xplore: 16 June 2020.

[27] H. Abdulmouti and E. Jassim, "Visualization and Measurements of Bubbly Two-Phase Flow Structure Using Particle Imaging Velocimetry (PIV)," European Scientific Journal (ESJ), /special/ edition No.3, ISSN: 1857 – 7431, pp. 197-208, June 2013.

[28] H. Abdulmouti. "Particle Imaging Velocimetry (PIV) Technique: Principles and Application," Yanbu Journal of Engineering and Science, 2.1, pp. 50-67, 2021.

[29]

[30] H. Abdulmouti, Y. Murai, J. Ohta, and F. Yamamoto, "Measurement of Bubble Plume Generated Surface Flow Using PIV," Journal of the Visualization Society of Japan, Vol. 21, No. 2, pp. 31-37, 2001.

[31] H. Abdulmouti, Y. Murai, J. Ohta, and F. Yamamoto, "PIV Measurement of Bubbly Flow Interaction with Water

Surface," Journal of the Visualization Society of Japan, Vol. 19, No. 2, pp. 209-210, 1999.

[32] H. Abdulmouti, Y. Murai, J. Ohta, and F. Yamamoto, "PIV Measurement of Surface Flow Induced by Bubble Curtain," Journal of the Visualization Society of Japan, Vol. 19. No. 1, pp. 239~242, 1999.

[33] H. Abdulmouti, Y. Murai, J. Ohta, and F. Yamamoto, "PIV Measurement and Numerical Analysis of Flow around Bubble Curtain," Japanese Society of Mechanical Engineer (JSME), No. 987-1, pp. 83-84, 1998.

[34] H. Abdulmouti, and T. Mohamed Mansour. "The Technique of PIV and Its Applications," 10th International Congress on Liquid Atomization and Spray Systems (ICLASS-2006), 27 Aug.-1 Sept. Kyoto, Japan.

 ISBN: 978-1-68558-054-4